

Article

Weak Fault Diagnosis Method of Rolling Bearings Based on Variational Mode Decomposition and a Double-Coupled Duffing Oscillator

Shijie Shan ^{1,*}, Jianming Zheng ¹, Kai Wang ¹, Ting Chen ¹ and Yuhua Shi ^{1,2}

¹ School of Mechanical and Precision Instrument Engineering, Xi'an University of Technology, Xi'an 710048, China; zjm@xaut.edu.cn (J.Z.); wangkai@xaut.edu.cn (K.W.); 1210210005@stu.xaut.edu.cn (T.C.); 228fly@sina.com (Y.S.)

² School of Equipment Management & Support, Engineering University of PAP, Xi'an 710078, China

* Correspondence: 1200210004@stu.xaut.edu.cn

Abstract: Aiming at the problems of the low detection accuracy and difficult identification of the early weak fault signals of rolling bearings, this paper proposes a method for detecting the early weak fault signals of rolling bearings based on a double-coupled Duffing system and VMD. The influence rule of system initial value on the response characteristics of a double-coupled Duffing system is studied, and the basis for its determination is given. The frequency of the built-in power of the system is normalized, and a variance evaluation standard for the output value of the double-coupled Duffing system for weak fault signals detection is established. In order to solve the interference problem of fault monitoring signals, VMD is proposed to pre-process the fault monitoring signals. The weak fault signal detection method proposed in this paper is tested and verified by simulation signals and rolling bearing fault signals. The results show that the method proposed in this paper can detect the weak fault signal with the lowest signal-to-noise ratio reduced by 2.96 dB compared with the traditional Duffing detection system, and it can accurately detect the early weak fault signal of rolling bearings.

Keywords: fault diagnosis; double-coupled Duffing system; VMD; variance



Citation: Shan, S.; Zheng, J.; Wang, K.; Chen, T.; Shi, Y. Weak Fault Diagnosis Method of Rolling Bearings Based on Variational Mode Decomposition and a Double-Coupled Duffing Oscillator. *Appl. Sci.* **2023**, *13*, 8505. <https://doi.org/10.3390/app13148505>

Academic Editor: Suchao Xie

Received: 15 June 2023

Revised: 16 July 2023

Accepted: 21 July 2023

Published: 23 July 2023



Copyright: © 2023 by the authors. Licensee MDPI, Basel, Switzerland. This article is an open access article distributed under the terms and conditions of the Creative Commons Attribution (CC BY) license (<https://creativecommons.org/licenses/by/4.0/>).

1. Introduction

The main task of weak signal detection is to extract weak signal features from strong background noise. In recent years, various weak signal detection methods have been widely used in radar detection, communication, fault diagnosis and other fields [1–3]. The commonly used detection methods mainly include wavelet decomposition, neural network detection, stochastic resonance, high-order spectral analysis, etc., which have good effects in signal noise reduction and feature extraction [4–10]. When the signal-to-noise ratio of the signal is too low, these methods often fail to show good performance. Such a problem also exists in the field of bearing fault diagnosis. Although the frequency of fault signals can be speculated, early weak fault signals are often buried in the complex background noise, which brings great difficulties to its fault diagnosis. As a common important part of mechanical equipment, the failure of bearings easily causes great economic losses and safety risks. Therefore, the feature extraction of weak signals is of great significance and is a major research direction for scholars in the field of signal processing.

A chaotic oscillator is widely used in signal processing because of its sensitivity to periodic signals and good anti-noise performance [11]. However, a signal detection method using a Duffing system has room for improvement. In recent years, many scholars have devoted themselves to the study of detecting weak periodic signals by using chaotic vibrators and achieved many achievements. In terms of the model of the system, a double-coupled Duffing system [12], a coupled Duffing and van der Pol–Duffing system [13] and a

double-coupled van der Pol–Duffing system [14] are proposed. By establishing a coupled system, there is a certain phase difference between the two coupled systems that can improve the anti-noise ability of the detection system. Scholars coupled the restoring force and damping terms of the system by studying the coupling items of the Duffing system and achieving certain improvement effects [15]. Some scholars modified the resilience items of the Duffing system and improved the detection performance of the Duffing system by using high-order resilience items [16]. When the Duffing system is used for fault detection, there is often a strong interference in the system, resulting in a low recognition rate.

When the Duffing system is used for signal detection, its chaos threshold needs to be judged. The commonly used methods to judge the chaos threshold include the Lyapunov index method, the correlation dimension method, the Melnikov index method, etc. [17]. After adding the signal to be tested into the Duffing system as an incentive, direct observation methods and the neural network learning discriminant method can be used to identify the state of the system [18,19]. These methods have a good effect, can effectively determine the chaos threshold and can judge the state of the system. In the aspect of system state recognition, there are a series of problems; for example, the efficiency of direct observation method may be not high, the neural network learning discriminant may have misjudgment, etc. These problems still need to be solved.

By preprocessing signals, the detection performance of chaotic systems can be effectively improved. Feature extraction is a commonly used preprocessing method, mainly including EMD, EWT, VMD, etc. [20–22]. Using these methods, the tested signal can be effectively decomposed into modal components, signal features can be extracted, and the impact of noise on signal detection can be reduced.

In order to improve the detection performance of existing methods, this paper proposes a method for the weak fault identification of rolling bearings based on VMD and a double-coupled Duffing system. Aiming at the problems of the low efficiency and low recognition rate of Duffing system state identification, according to the different motion characteristics of the output value of a Duffing system in a chaotic state and large-scale periodic state, this paper proposes a method of state identification by using the variance of the displacement output value of the Duffing system. Aiming at the problem of poor stability in the early stage of the Duffing system, the initial value of the system is determined by combining the variance of the output value so that the system output is convenient for phase identification. Aiming at the problem of the Duffing system's common interference via noise and other frequency signals, a method is proposed to extract the features of signals by using VMD and then to analyze the extracted signals by using the Duffing system. The method proposed in this paper can detect bearing faults with characteristic frequencies (inner ring faults, outer ring faults, rolling element faults, retainer faults, etc.). Simulation signals were used to evaluate the proposed method, its detection capability was judged, and the effectiveness of the proposed method was verified by experimental data.

2. Materials and Methods

This paper proposes a new method for early weak fault signal diagnosis of rolling bearings. Firstly, the improved VMD method is used to preprocess the signal. Then, the processed signal is used as the excitation for the improved double-coupled Duffing system. Finally, based on the output of the double-coupled Duffing system and the variance judgment index established in this paper, we determine whether the fault exists.

For the double-coupled Duffing system, the main work of the study involves threshold determination, state discrimination, initial value optimization, variable scale, phase shift, amplitude normalization and sweep detection. The main task for the VMD algorithm is to determine the number of IMFs. The specific implementation process will be described in detail below.

3. The Mathematical Model of Double-Coupled Duffing System

3.1. Holmes–Duffing System

The Duffing system was first proposed by BIRX D and PIPENBERG S et al. [23]. As a nonlinear dynamic system. The Duffing system has a simple structure but rich dynamic behavior, which is widely used by scholars in various fields. The physical model of the traditional Holmes–Duffing oscillator (hereinafter referred to as the Duffing system) is shown in Figure 1.

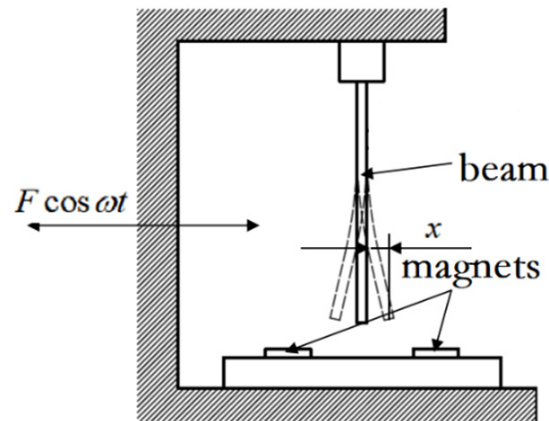


Figure 1. Physical model of the Duffing system.

As shown in Figure 1, the structure of the model is mainly composed of two electromagnets and a cantilever beam, and the electromagnet is fixed on a sliding table. The end of the cantilever beam is recorded as the displacement of the oscillator. When the cantilever beam is not deformed, the horizontal position directly below it is the origin of the displacement. After the electromagnet is energized, the cantilever beam is deformed under force, and there is a stable point on the left and right sides. The displacement of the left stable point is recorded as -1 , and the displacement of the right stable point is recorded as 1 . Assuming that the sliding platform moves in the way of $F\cos(\omega t)$, the mathematical model of the traditional Holmes–Duffing system shown in Equation (1) below can be established.

$$\ddot{x} + \zeta\dot{x} - x + x^3 = F\cos(\omega t) \quad (1)$$

where, \ddot{x} , \dot{x} , x are the acceleration, velocity and displacement of the vibrator, and ζ is the damping ratio of the system. In this paper, the value of ζ is 0.5 , $F\cos(\omega t)$ is the elastic restoring force of the system, F is the amplitude of the built-in driving force, and ω is the frequency of the built-in driving force.

3.2. The Mathematical Model of Double-Coupled Duffing System

The double-coupled Duffing system is a coupled nonlinear dynamic equation established by two Duffing systems. By introducing coupling terms, it makes a certain phase difference between the two systems and improves the anti-noise performance of the system. Coupling item generally refers to coupling damping or the nonlinear items of two Duffing systems. Scholars in various fields have studied different coupling forms, and some scholars have explored triple-coupled Duffing systems, all of which have achieved certain results [24].

In this paper, the displacement of the vibrator is selected as the coupling term to establish a double-coupled Duffing system, and its mathematical model is shown in Equation (2):

$$\begin{cases} \ddot{x} + \zeta\dot{x} - x + x^3 + k(x - y) = F\cos(\omega t) \\ \ddot{y} + \zeta\dot{y} - y + y^3 + k(y - x) = F\cos(\omega t) \end{cases} \quad (2)$$

where k is the coupling coefficient; x, y , respectively, represent the displacement of two Duffing systems; \ddot{y}, \dot{y}, y are the acceleration, velocity and displacement of the second Duffing system.

When k is 0, the two Duffing systems lose their association, and the output of the double-coupled Duffing system is exactly the same as that of the single Duffing system. When k is not 0, the actions of the two Duffing systems tend to be synchronized and have similar motion trajectories under the action of the coupling term.

Some research has shown that, when the k value is 2, the system can show good stability [25], so in this paper, k is taken as 2.

3.3. Response Characteristics and Weak Signal Detection Principle of Double-Coupled Duffing System

With the displacement of the vibrator as the abscissa and the velocity as the ordinate, the phase trajectory diagram of the Duffing system response can be drawn. The Duffing system will show the attractor, homoclinic orbit, periodic bifurcation, chaotic state, large-scale periodic state and other states in the phase trajectory as the amplitude of the built-in power increases. The double-coupled Duffing system is composed of two Duffing systems, and each Duffing system corresponds to a phase plane diagram. Because the phase trajectories of the two Duffing systems are similar, only one of them is calculated during analysis.

Set the frequency of the built-in power to 1 rad/s. ODE45 is used to solve the response of the double-coupled Duffing system. The discrete time interval t_s is taken as 0.1 s. In Figure 2, the evolution law of the phase trajectory and the time domain waveform of the first Duffing system response with the amplitude change of the built-in power is shown.

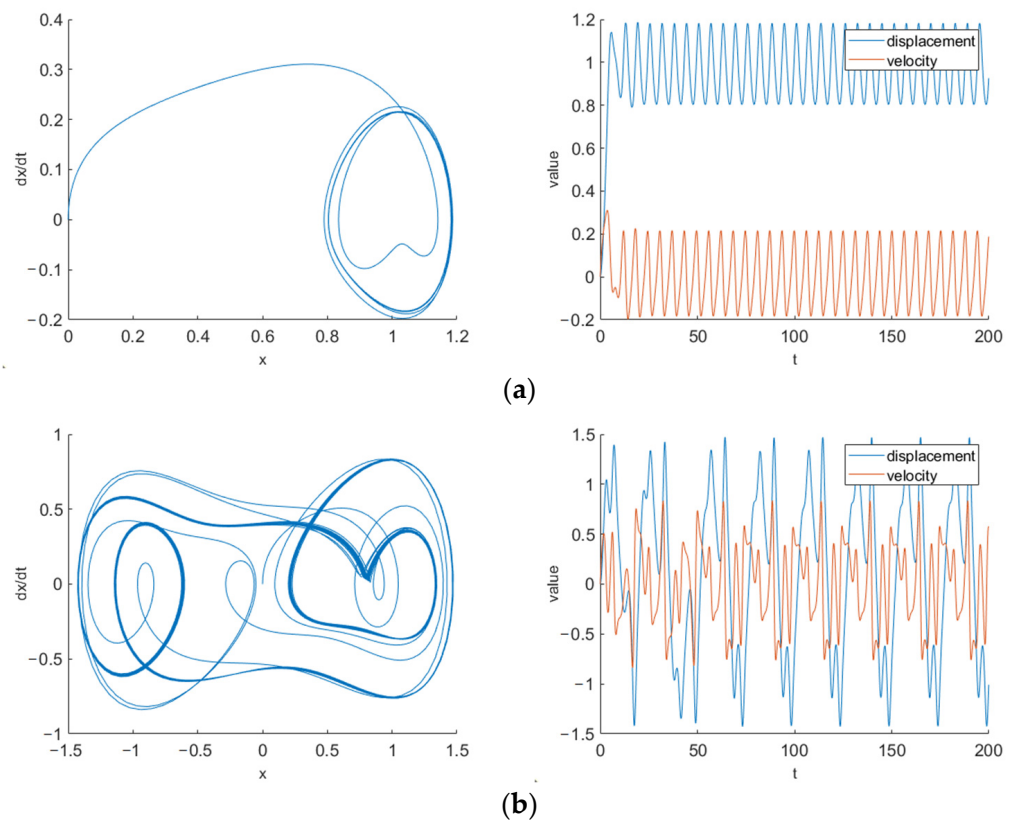


Figure 2. Cont.

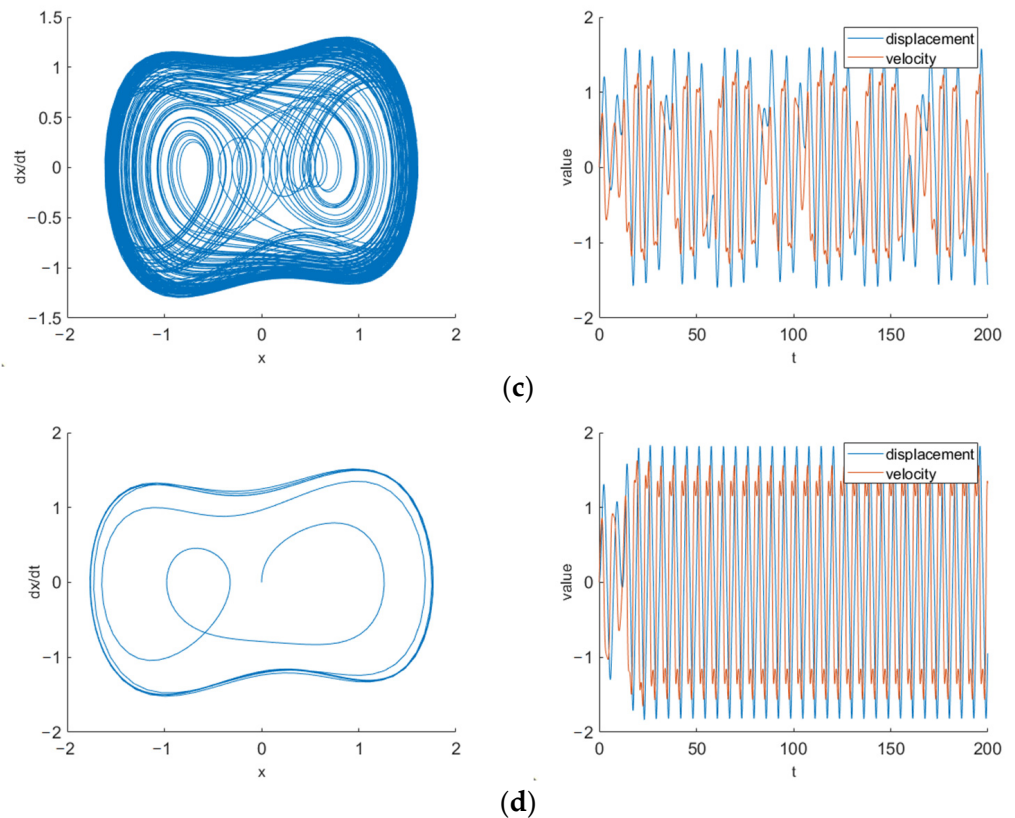


Figure 2. Phase plane diagram and domain diagram of Duffing system. (a) $F = 0.2$, homoclinic orbit; (b) $F = 0.5$, periodic bifurcation; (c) $F = 0.8$, chaotic state; (d) $F = 1$, large-scale periodic state.

According to the phase trajectory and time domain waveform evolution law in Figure 2, the double-coupled Duffing system shows different types of dynamic response characteristics with the increase in the amplitude of the built-in power. There are critical points between the states. When the amplitude of the built-in force is at the critical point, a small increment will cause a sudden change in the system response state. Therefore, when there is a weak component in the signal to be measured with the same frequency as the built-in force, superposing it with the built-in force into the double-coupled Duffing system will cause a sudden change in the system response so as to achieve weak signal detection. The research shows that the Duffing system is insensitive to signals with different frequencies from the built-in driving force and has excellent weak signal detection ability and anti-noise performance.

4. Establishment of Double-Coupled Duffing Weak Signal Detection System

4.1. Variance Discriminant Method for Response State of Double-Coupled Duffing System

It can be seen from the response of the above double-coupled Duffing system under the action of different amplitude built-in forces that its phase diagram and time domain diagram are very complex, and it is difficult to determine the judgment criteria for different states and critical points. According to the distribution characteristics of phase diagram trajectories in different states of the double-coupled Duffing system, this paper proposes to use the variance of the output phase trajectories of the double-coupled Duffing system as the basis for system state determination. The variance definition and calculation equation of the output phase trajectory value of the double-coupled Duffing system is as follows:

$$D_{output} = \frac{\sum_{i=1}^M \left((x_{1,i} - \bar{x}_1)^2 + (x_{2,i} - \bar{x}_2)^2 \right)}{M} \tag{3}$$

where i is the number of sampling points for the output phase trajectory, $x_{1,i}$ and $x_{2,i}$ are the displacement and velocity output values of the first Duffing system at the i th sampling time, and \bar{x}_1 , \bar{x}_2 are the mean values of displacement and velocity output values of the first Duffing system, respectively.

Figure 3 shows the variation in the variance output value with the amplitude of the built-in force. The red dashed line in the figure represents the critical point between different states. When a double-coupled Duffing system enters a large periodic state from a chaotic state, the phase trajectory variance usually jumps significantly. According to this change feature of variance, this paper defines the following variance jump rate to determine whether the system state jumps:

$$R = \frac{s_t^2 - s_2^2}{s_1^2 - s_2^2} \quad (4)$$

where R is the variance jump rate, s_1^2 is the variance of the output phase trajectory after the system enters the large periodic state, s_2^2 is the variance of the system at the chaotic threshold (the critical point of the chaotic state and the large-scale periodic state), and s_t^2 is the variance of the output phase trajectory of the system excited by the signal to be measured.

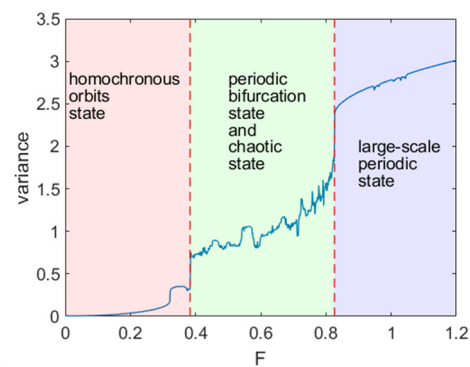


Figure 3. Variation of the variance output value with the amplitude of the built-in force.

When the variance jump rate is greater than a certain value, it is considered that a state jump has occurred at this time. This value is called the variance jump rate threshold. The determination of the size of the variance jump rate threshold is the key to this decision method. If the threshold is set too high, the detection performance of the Duffing system will be reduced, and if the threshold is set too low, the robustness of the Duffing system detection will be reduced. After a lot of simulation tests, the variance jump rate threshold is set to 0.8.

4.2. Determination of Chaotic Threshold of Double-Coupled Duffing System

According to the above weak signal detection principle of the double-coupled Duffing system, the amplitude of the built-in power needs to be adjusted to the chaos threshold first. There are many factors that affect the chaos threshold of the double-coupled Duffing system, such as the solution method, the calculation step, the initial value of the system, etc.

In this paper, the maximum Lyapunov exponent is used to determine the chaos threshold of the double-coupled Duffing system. The coupling term of the double-coupled Duffing system will make the two Duffing systems related, which will cause a weak difference in response and have a certain impact on the chaos threshold, but this impact is extremely weak and can be ignored. Therefore, the chaos threshold of a single Duffing system is used as the chaos threshold of the double-coupled Duffing system in this paper. For a single Duffing system, there are two Lyapunov exponents, the larger of which is the maximum Lyapunov exponent. The maximum Lyapunov exponent will change from a positive value to a negative value if and only if the system moves from a chaotic state to a

large-scale periodic state with the amplitude change in the built-in power. According to this feature, by increasing the amplitude of the built-in power, when the maximum Lyapunov exponent changes from a positive value to a negative value, the amplitude of the built-in power corresponding to the last positive Lyapunov exponent is the chaos threshold.

Under the system parameters in this paper, the frequency of the built-in force is set as 1 rad/s. According to the above calculation method, when the amplitude of the built-in force is 0.826, the maximum Lyapunov index is positive, and the system is in a chaotic state. When the amplitude of the built-in force is 0.827, the maximum Lyapunov index is negative, and the system is in a large-scale periodic state. Therefore, the chaotic threshold of the system is 0.826. The phase trajectory diagram when the built-in force is 0.826 and 0.827 is shown in Figure 4.

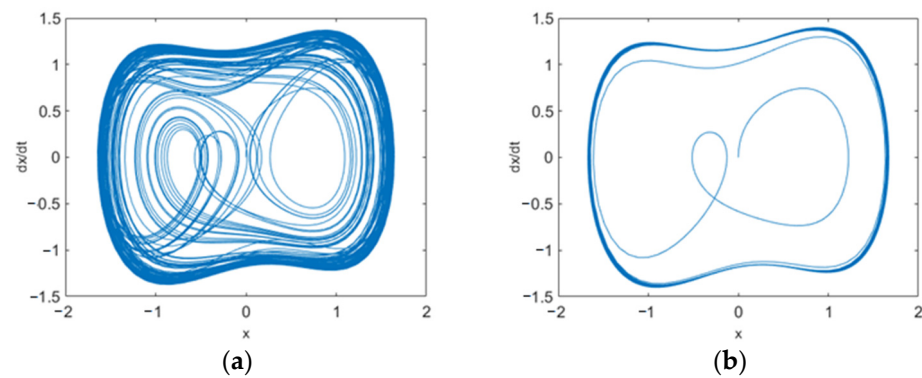


Figure 4. Phase trajectories of different states. (a) $F = 0.826$; (b) $F = 0.827$.

4.3. Determination of Chaotic Threshold of Double-Coupled Duffing System

First, under any initial value, adjust the built-in force of the system to make the system in a large-scale periodic state and record the track range of periodic motion at this time. Then, traverse the initial value points within this range and calculate whether it can make the variance of the system’s output value increase steadily with the growth of the built-in force. The calculation method is shown in Equations (5) and (6):

$$Y = \sum_{n=0}^{m-1} sp(D(F_0 + nd) - D(F_0 + (n - 1)d)) / m \tag{5}$$

$$sp(x) = \begin{cases} 1 & x > 0 \\ 0 & x \leq 0 \end{cases} \tag{6}$$

where Y is the fluctuation index, $sp(x)$ is a judgment function, m is the number of calculations, $D(F)$ is the variance of the output value of the double-coupled Duffing system when the amplitude of built-in force is F , F_0 is the chaos threshold and can be calculated by the method shown in Section 4.2, and d is the calculation step of the amplitude of the built-in force. The Y value essentially reflects the fluctuation of the variance of the output value of the double-coupled Duffing system when the built-in driving force increases from the chaos threshold to $F_0 + md$. If it is 0, it means that the variance of the output value of the system increases steadily with the increase in the built-in driving force. The larger the Y value, the greater the fluctuation in the variance of the output value.

After traversing the initial value points within the calculation range, we can obtain regions that can make the variance of the output value increase steadily. As shown in Figure 5, The red area is stable, select points close to the large periodic orbit as the initial value of the system in these regions. At these locations, the oscillator can quickly enter the orbit, which is conducive to the identification of the system state. According to the calculation results in Figure 5, the initial values of velocity and displacement selected in this paper are 1.2 and 0, respectively. Under this initial value, the chaos threshold is calculated

according to Section 4.2, and the chaos threshold at this time is 0.825. In this paper, the variance of the output value when the built-in force is 0.825 is selected as s_2^2 ; its value is 2.0333. The variance of the system output value when the built-in force is 0.826 is selected as s_1^2 ; its value is 2.4028. According to the criteria in Section 4.1, when the double-coupled Duffing system is excited by the signal to be tested, if its square difference jump rate exceeds 0.8, that is, the variance of the output value exceeds 2.3289, it can be considered that the signal to be tested has been detected.

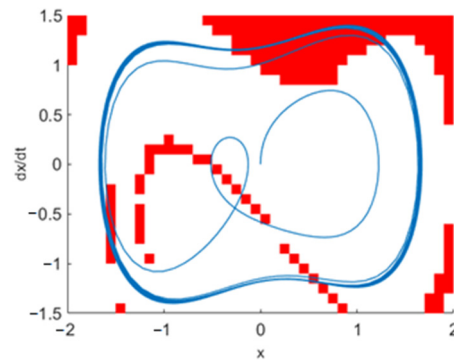


Figure 5. Output value variance stable region distribution map.

4.4. Variable Scale and Phase Shift Processing of Double-Coupled Duffing System

In order to facilitate the detection of any frequency signal in engineering applications, the time variable τ is introduced to rewrite the mathematical model of a Duffing system. The time scale is transformed as follows [26]:

Define $t = \omega\tau$, where τ is a generalized time variable. Then,

$$\dot{x}_1 = \frac{dx}{dt} = \frac{1}{\omega} \frac{dx}{d\tau} \quad \dot{x}_2 = \frac{1}{\omega^2} \frac{dx^2}{d\tau^2} \tag{7}$$

Then, rewrite τ as t , and Equation (3) can be rewritten as:

$$\begin{cases} \dot{x}_1 = \omega x_2 \\ \dot{x}_2 = \omega [-\zeta x_2 + x_1 - x_1^3 + k(y_1 - x_1) + F\cos(\omega t) + A(t)] \\ \dot{y}_1 = \omega y_2 \\ \dot{y}_2 = \omega [-\zeta y_2 + y_1 - y_1^3 + k(x_1 - y_1) + F\cos(\omega t)] \end{cases} \tag{8}$$

After this change, the Duffing system can detect signals of any frequency without changing the chaotic threshold. When detecting signals of different frequencies, it is only needed to modify the parameter ω to the frequency to be measured. It is unnecessary to calculate the chaotic threshold according to the frequency of the built-in force. The chaos threshold of the system will not change, and its value is the chaos threshold when the built-in power frequency is 1 rad/s.

When the Duffing system is used to detect the signal to be measured, sometimes the frequency of the signal to be measured is equal to the frequency of the built-in driving force of the system, but the state of the system does not change. This is due to the phase difference between the signal to be measured and the built-in driving force of the system [27]. If the phase difference between the signal to be measured and the built-in driving force of the system is φ , the total excitation of the system is

$$F_{sum} = A_0\cos(\omega t) + A\cos(\omega t + \varphi) = \sqrt{A_0^2 + 2A_0A\cos\varphi + A^2}\cos[\omega t + \theta(t)] \tag{9}$$

where F_{sum} is the total driving force of the Duffing system, A_0 is the amplitude of the built-in driving force of the Duffing system, A is the amplitude of the signal to be measured, and $\theta(t)$ is the phase difference between the total driving force and the built-in driving force.

Make the total driving force greater than the chaos threshold. Because $A_0 \gg A$, when φ is in the range of $(-\pi/2, \pi/2)$, the amplitude of the total driving force of the system is greater than the chaos threshold. At this time, it can be detected correctly. Otherwise, the same frequency signal will reduce the amplitude of the total driving force, causing false detection.

According to the above analysis, a single calculation cannot detect the signal to be measured at any initial phase angle, and multiple calculations are required. In order to eliminate the detection blind area so that multiple calculations can detect the full range of phase angles, different initial phase angles can be used, or the signal to be measured can be phase-shifting. Since two calculations can cover all phase angles, this paper uses the method of two calculations to shift the phase of the signal to be measured. In the first calculation, the signal to be measured is not processed. In the second calculation, the signal is inversed as a whole, which is equivalent to adding a phase angle of π to the signal. In this way, the second calculation can detect the detection blind area in the first calculation, thus avoiding misjudgement.

If the same frequency signal is included, one of the two calculations will make the state of the double-coupled Duffing system jump. Therefore, after the two variance jump rates are calculated, the maximum variance jump rate is retained. If the maximum variance jump rate is greater than the jump rate threshold, it is proved that the same frequency signal is detected.

4.5. Amplitude Normalization and Sweep Detection of Double-Coupled Duffing System

In practical engineering applications, the value size of the collected sensor data will be different, and the signal with unreasonable energy size will make the system unable to detect normally. Before detection, it is necessary to normalize the signal amplitude. In this paper, after extensive simulation calculations, the energy of the signal to be measured is normalized to the same as the white noise with a variance of 0.01. At this amplitude, the double-coupled Duffing system has good detection performance for periodic signal components in the tested signal.

When the double-coupled Duffing system is used for signal detection, a certain frequency difference is allowed between the signal to be measured and the built-in policy force of the system, so the Duffing system can detect a signal in a narrow frequency band each time. The width of this frequency band is related to the amplitude of the signal to be measured: the larger the amplitude, the wider the frequency band. For weak periodic signals with an amplitude of 0.001, the band width that can be detected is 0.003ω , where ω is the frequency of the signal to be measured. In order to ensure the robustness of the algorithm, the sweep step is set to 0.002ω . When using the double-coupled Duffing system for bearing fault diagnosis, the bandwidth is used as the step size for frequency scanning to realize fault signal identification. Due to the complex working conditions in the actual machining process, there may be a certain deviation between the actual fault signal frequency and the theoretical value, but this deviation is very small. Therefore, when carrying out bearing fault diagnosis, it is only necessary to sweep the frequency of the neighborhood of the calculated theoretical value to complete the fault identification, which greatly reduces the amount of calculation and is conducive to the establishment of the real-time monitoring system.

5. Variational Modal Decomposition

5.1. Problems in Weak Signal Detection of Double-Coupled Duffing System

In practical engineering problems, the acquired signals are often complex and contain many components, such as working frequency, natural frequency, fault frequency, etc. The component of fault frequency usually has weak energy, and the energy of other components is relatively strong. When the double-coupled Duffing system is used for diagnosis, other high-energy components and noises in the signal will have a certain impact on the detection. The noise will cause the trajectory of the vibrator to fluctuate, which is shown in the phase

trajectory diagram as the distance between the inner and outer contours of the long-period orbit becomes larger. The effect of the high energy component is the deformation and distortion of the phase trajectory. Its essence is that the high energy makes the response of the double-coupled Duffing system appear obvious with components that have the same frequency as this component, which will cause the trajectory deformation after superposing with the components of the frequency to be measured. In extreme cases, if the amplitude of the high-energy component of the frequency not to be measured exceeds the chaos threshold corresponding to the frequency, then, regardless of whether there is a component with the same frequency as the built-in policy force, the double-coupled Duffing system will enter a large-scale periodic state, resulting in false detection.

To solve this problem, the feature extraction method is considered to extract the feature of fault frequency to eliminate the influence of other frequency components on the double-coupled Duffing system. In this field, VMD is widely used and is better than other algorithms. Therefore, this paper uses the VMD algorithm to pre-process data.

5.2. Variational Modal Decomposition Process

VMD (variational mode decomposition) is a signal feature extraction algorithm with excellent performance. It can decompose the signal into several components with limited bandwidth. Compared with EMD (empirical mode decomposition), this method has the advantage of effectively reducing frequency aliasing [27]. For weak fault signals of early bearings, if frequency aliasing occurs, the energy of the periodic signal in the test signal will be dispersed into the adjacent two IMFs, making it more difficult for the double-coupled Duffing system to detect periodic signals. However, VMD also has certain defects. The adaptability of its algorithm is weaker than other algorithms. The number of mode components (IMF) generated by its decomposition is usually determined by manual setting. If the number of IMFs is too small, frequency aliasing will occur. If the number of IMFs is too much, More useless components will be generated, so the number of IMFs is particularly critical.

The eigen modal components obtained by VMD algorithm decomposition can be expressed by Equation (10) [28]:

$$u_k(t) = A_k(t)\cos\varphi_k(t) \tag{10}$$

where $u_k(t)$ is the k th eigenmode function obtained by decomposition, $u_k(t)$ satisfies $\sum_{k=1}^K u_k = f(t)$, $f(t)$ is the signal before decomposition, K is the total number of eigenmode functions to be decomposed, $A_k(t)$ is the instantaneous amplitude, and $\varphi_k(t)$ is the instantaneous phase. The instantaneous frequency is the derivative of the instantaneous phase, and the values of the instantaneous amplitude and the instantaneous frequency are positive real numbers.

The VMD algorithm has completed the solution of a variation problem: $u_k(t)$ is transformed by Hilbert transform to obtain its unilateral spectrum, and each IMF is modulated to the response fundamental frequency band via exponential mixed modulation. Finally, Gaussian smoothing is used to demodulate, and the bandwidth of $u_k(t)$ is estimated. The variation model to be solved is as follows:

$$\min_{\{u_k\},\{\omega_k\}} \left\{ \sum_{k=1}^K \left\| \partial_t \left[\left(\delta(t) + \frac{j}{\pi t} \right) * u_k(t) \right] e^{-j\omega_k t} \right\|^2 \right\} \tag{11}$$

where ω_k is the center frequency corresponding to each u_k , and $\delta(t)$ is the unit pulse function. The penalty factor α and the Lagrange multiplier λ are introduced into the model. By introducing the penalty factor, the fidelity of the reconstructed signal can be guaranteed. The larger the value is, the smaller the bandwidth of the decomposed frequency band will be. If the bandwidth is too small, the signal will be lost. By introducing Lagrange

multipliers, the strictness of the constraint conditions can be guaranteed. After modification, the constrained variational problem is changed into an unconstrained variational problem:

$$\begin{aligned}
 L(\{u_k\}, \{\omega_k\}, \lambda(t)) &= \alpha \sum_{k=1}^K \left\| \partial_t \left[(\delta(t) + \frac{j}{\pi t}) * u_k(t) \right] e^{-j\omega_k t} \right\|_2^2 \\
 &+ \left\| f(t) - \sum_{k=1}^K u_k(t) \right\|_2^2 + \langle \lambda(t), f(t) - \sum_{k=1}^K u_k(t) \rangle
 \end{aligned} \tag{12}$$

where α is the bandwidth coefficient, and $\lambda(t)$ is the Lagrange multiplier.

The ADMM method is used to update $\hat{u}_k^{n+1}, \hat{\omega}_k^{n+1}, \hat{\lambda}_k^{n+1}$ iteratively. After meeting the iteration termination conditions, K IMF components obtained by decomposition can be output. The process is as follows:

1. Initialize $\{\hat{u}_k^1\}, \{\hat{\omega}_k^1\}, \hat{\lambda}^1$ and set n to 0;
2. Let $n = n + 1$, and when $\omega \geq 0$, update $\hat{u}_k, \hat{\omega}_k$:

$$\hat{u}_k^{n+1}(\omega) = \frac{\hat{f}(\omega) - \sum_{i \neq k} \hat{u}_i(\omega) + \frac{\hat{\lambda}(\omega)}{2}}{1 + 2\alpha(\omega - \omega_k)^2} \tag{13}$$

$$\omega_k^{n+1} = \frac{\int_0^\infty \omega |\hat{u}(\omega)|^2 d\omega}{\int_0^\infty |\hat{u}(\omega)|^2 d\omega} \tag{14}$$

3. Update λ :

$$\hat{\lambda}^{n+1}(\omega) = \hat{\lambda}^n(\omega) + \tau(\hat{f}(\omega) - \sum_{k=1}^K \hat{u}_k^{n+1}(\omega)) \tag{15}$$

4. Determine whether the iteration conditions are met according to Equation (16). If yes, stop the iteration and output the final results. If not, return to step 2 and perform the next iteration calculation.

$$\sum_{k=1}^K \left\| \hat{u}_k^{n+1} - \hat{u}_k^n \right\|_2^2 / \left\| \hat{u}_k^n \right\|_2^2 < \varepsilon \tag{16}$$

5.3. Determination of IMF Quantity of VMD

The VMD algorithm can decompose the signal into a specified number of IMF components. In terms of setting the number of IMF components, this paper uses the EMD algorithm to determine this number. Because the EMD method has good adaptability, this algorithm can generate a moderate number of IMF components according to the complexity of the signal. This paper executes the EMD algorithm on this time series after obtaining the signal to be tested. Take the number of IMF components decomposed by the EMD algorithm as the number of IMF components to be decomposed by the VMD algorithm and then execute the VMD algorithm. This method can effectively avoid overdecomposition and information loss.

For the early weak fault diagnosis of rolling bearings, the energy of fault signal frequency may be too weak to overlap with the center frequency of an IMF obtained after VMD decomposition. In response to this phenomenon, this article superimposes two IMF components with a center frequency near the fault frequency. Via this processing, the impact of other frequency noises on the detection system can be reduced while ensuring that the frequency characteristics of the signal to be tested are retained.

6. Simulation and Experiment of Weak Signal Detection Using Double-Coupled Duffing System

6.1. Simulation Study of Single-Component Noisy Signal Detection

In order to verify the detection ability of the method proposed in this paper, a single-component noisy signal is used for testing. The composition of the signal is shown in Equation (17):

$$A_s(t) = A\cos(\omega t) + n(t) \tag{17}$$

where $A\cos(\omega t)$ is the periodic signal with amplitude A and frequency ω , and $n(t)$ is the white noise with a variance of 0.01.

Set the frequency of the periodic signal to 1 rad/s and use the method in Section 3.3 to detect the single-component signal in Equation (17). Since the signal has only one significant component, and there is no phase difference between the component and the built-in driving force, and the frequency is the same, there is no need to carry out frequency normalization, phase shift, VMD decomposition and other operations. When the amplitude of the periodic signal in the single-component noisy signal is 0.006, the signal to be measured is used to excite the traditional Holmes–Duffing system and the double-coupled Duffing system established in this paper, and the phase plane diagram of the system output is shown in Figure 6.

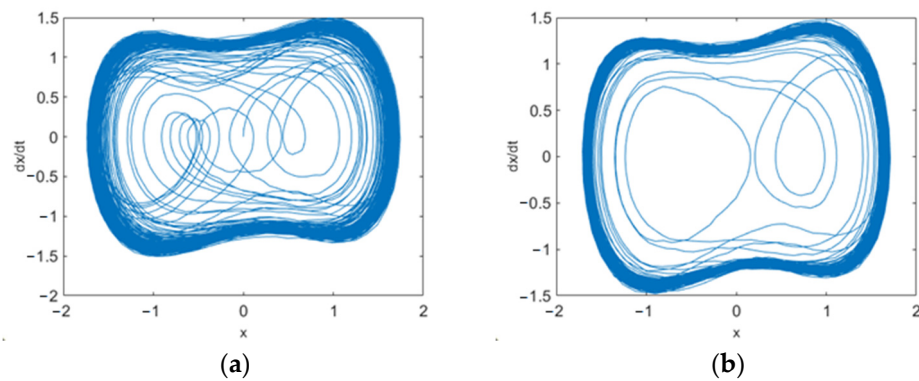


Figure 6. Phase plane diagram of Duffing system. (a) Holmes–Duffing system; (b) double-coupled Duffing system.

According to Figure 6, by comparing the phase plan, it is found that the double-coupled Duffing system is in the large-period state, and the variance of the output value of the system is 2.3415. Although there is irregular movement in some periods, by calculating the variance jump rate, according to the criteria proposed in this paper, it can be considered that the signal to be tested is detected at this time. However, the Holmes–Duffing system is still in chaos under the same excitation, the output value variance is only 2.2198, and its variance jump rate does not exceed the threshold, so it is considered that the signal to be measured is not detected at this time. The above analysis proves that the double-coupled Duffing system established in this paper has better anti-noise performance.

In order to calculate the detection capability of the proposed method, it is necessary to calculate the lowest signal-to-noise ratio that can be detected by the method. The equation for calculating the signal-to-noise ratio is shown in Equation (18).

$$SNR = 10 \lg \frac{A^2}{2\delta^2} \tag{18}$$

where SNR is the signal-to-noise ratio of the signal, and δ is the standard deviation of white noise.

Calculate the simulated signal of Equation (17), constantly modify the amplitude of the periodic signal, calculate 100 times for each amplitude strength, count the output value variance of the double-coupled Duffing system, and draw the box-type diagram as

shown in Figure 7. It can be seen from Figure 7 that, with the increase in the amplitude of the periodic signal, the variance of the output value is on the rise as a whole, and the distribution is more concentrated. According to the analysis in the second chapter, it is considered that the signal to be measured is detected when the variance of the output value is greater than 2.3289. According to this standard, combined with statistical analysis, the double-coupled Duffing system established in this paper has the ability to detect signals with a signal-to-noise ratio of -23.74 dB.

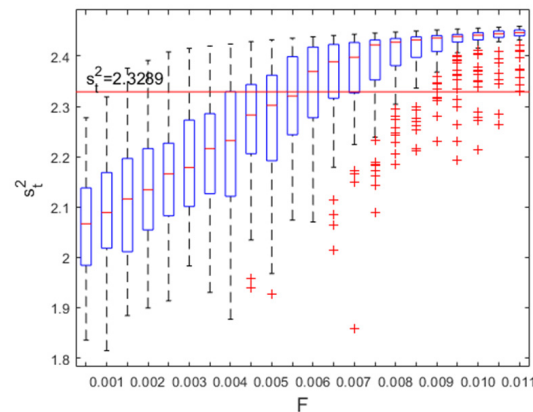


Figure 7. Box graph of output value variance of double-coupled Duffing system.

Starting from 0, gradually increase the amplitude of the periodic signal in steps of 0.0001 and repeat the calculation 100 times for each amplitude of the signal. To ensure the rationality of the simulation experiment, 100 random number seeds were generated before calculation, and white noise in 100 repeated calculations under all periodic signal amplitudes was generated using these 100 random number seeds. The traditional Holmes–Duffing system and the double-coupled Duffing system established in this article were tested separately, and the recognition rate varies with the amplitude of the periodic signal in the tested signal as shown in Figure 8.

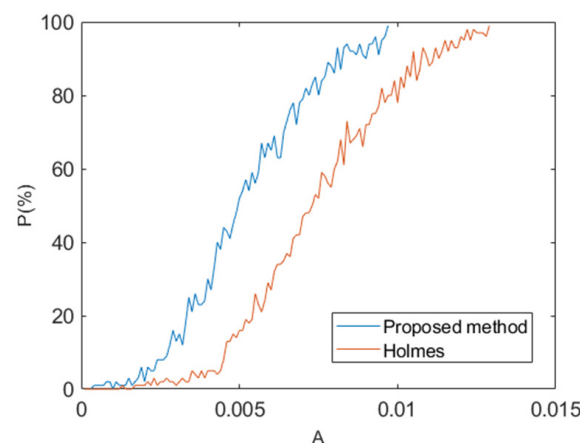


Figure 8. Recognition rate variation chart.

Observing Figure 8, the recognition rate of the method proposed in this paper is significantly better than that of the traditional Holmes–Duffing system. After calculation, the minimum signal-to-noise ratio that the traditional Holmes–Duffing system can detect is -20.80 dB. Via this analysis, it is shown that the double-coupled Duffing system established in this article has a 2.96 dB decrease in the minimum signal-to-noise ratio that can be detected compared to the Holmes–Duffing system, and it has better detection performance.

6.2. Simulation Study of Multi-Component Noisy Signal Detection

In this section, the multi-component signal is used for simulation and research. A multi-component noisy signal is constructed as shown in Equation (19):

$$A_{test}(t) = 0.01(\cos(10t)) + 0.5(\cos(50t)) + n(t) \quad (19)$$

Detect the 10 rad/s component in the signal and set the ω parameter in the detection system to 10 according to the method in Section 4.4. Without introducing the VMD decomposition, directly excite the double-coupled Duffing system, and obtain the phase plane as shown in Figure 9.

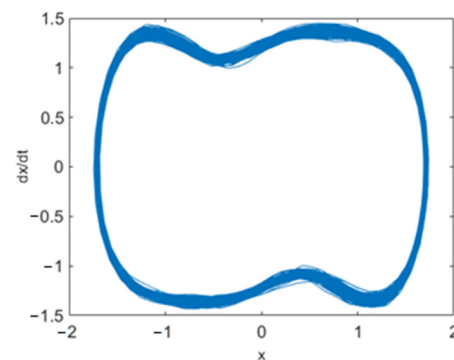


Figure 9. Phase plane diagram of Duffing system (The signal contain a frequency component of 10 rad/s).

As shown in Figure 9, it can be observed that the double-coupled Duffing system is in a large-scale periodic state. At this time, the variance of the output value of the system is 2.5125. According to the judgment method in Section 4.3, its variance jump rate has exceeded the threshold, and it can be considered that the signal to be measured has been detected, but at the same time, it can also be observed that, due to the interference of other frequency components with high energy, the phase plane trajectory of the system has been deformed, which will affect the detection performance. Delete the periodic signal component of 10 rad/s in Equation (19) and excite the double-coupled Duffing system again to obtain the phase plan as shown in Figure 10.

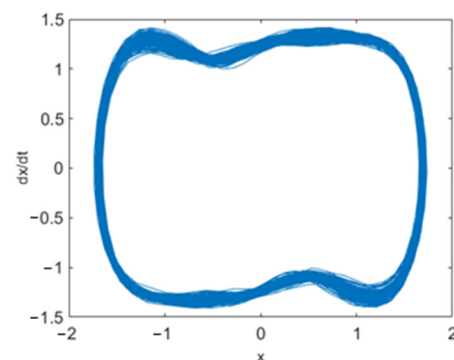
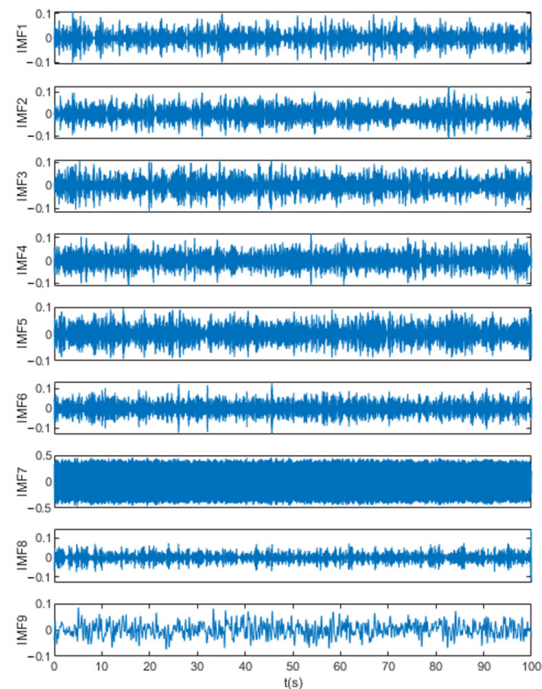


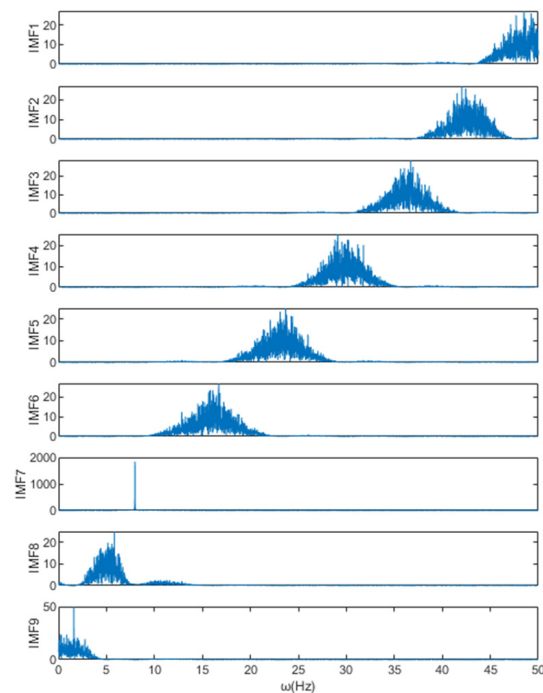
Figure 10. Phase plane diagram of Duffing system (The signal does not contain a frequency component of 10 rad/s).

It can be seen from Figure 10 that the system is still in a large-scale periodic state after deleting the components of the frequency to be measured, which indicates that the system has lost its due detection ability under the interference of high-energy signals from other components.

According to the method in Section 4.3, the signal is first decomposed by EMD, and nine IMF components are obtained after EMD decomposition. Set the number of IMF components of the VMD algorithm to 9 and perform VMD decomposition. The IMF components and their center frequencies are obtained as shown in Table 1. The time domain diagram and frequency domain diagram of each IMF are shown in Figure 11.



(a)



(b)

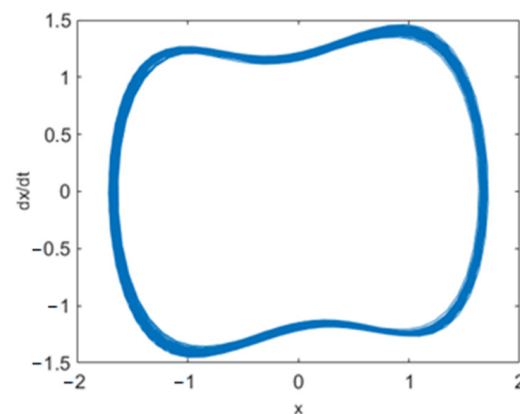
Figure 11. VMD decomposition results. (a) Time domain diagram of VMD decomposition; (b) frequency domain diagram of VMD decomposition.

Table 1. VMD decomposition results (simulated signals).

IMF	Center Frequency (rad/s)	IMF	Center Frequency (rad/s)
IMF1	302.640	IMF6	100.869
IMF2	268.330	IMF7	50.044
IMF3	227.802	IMF8	32.374
IMF4	187.232	IMF9	9.468
IMF5	146.385		

By observing Table 1 and Figure 11, it can be seen that the center frequency of IMF7 coincides with the frequency of the high-energy component in the signal. The high-energy component can be clearly observed in IMF7, the frequency component to be measured can be observed in IMF9, and other components are useless noise components. According to the calculated center frequency of each component, the frequency to be measured is greater than the center frequency of IMF9 and less than the center frequency of IMF8. IMF8 and IMF9 are extracted and superimposed. After this operation, the high-energy frequency components in IMF7 are eliminated.

Take the extracted features as the input of the double-coupled Duffing system and obtain the phase plane of the system output as shown in Figure 12.

**Figure 12.** Phase plane diagram of Duffing system (processed by VMD).

By observing Figure 12, the system is in a large-period state at this time, which proves that the system has detected the signal to be measured. Compared with the phase plane in Figure 9, the phase plane at this time is smoother, which greatly alleviates the problem of phase track ambiguity and deformation, which is beneficial for phase state discrimination. In order to fully prove the improvement of VMD decomposition on the detection performance of the double-coupled Duffing system, the frequency component of 10 rad/s in the signal to be measured is deleted. After the above steps are repeated, the double-coupled Duffing system is excited, and the phase plane is obtained as shown in Figure 13.

It can be seen from Figure 13 that, after the frequency component to be measured is deleted, the system is in a chaotic state, which proves that the signal component to be measured is not detected at this time. Compared with the results in Figure 11, it can be proved that the introduction of the VMD method to signal pre-processing can effectively reduce the impact of other components on the double-coupled Duffing system and improve the detection performance of the system.

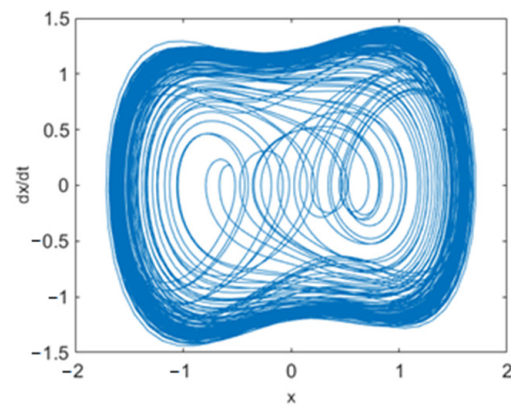


Figure 13. Phase plane diagram of Duffing system (without VMD processing).

6.3. Experimental Study on Weak Fault Signal Detection of Rolling Bearing

In the previous section, the simulation signal is used to verify the method proposed in this paper. In order to verify the performance of the method in practical engineering applications, it is necessary to test it with the measured signal. In this paper, the bearing failure data of Case Western Reserve University is used. This dataset covers normal data and four types of fault data (inner ring faults, outer ring faults, rolling element faults and retainer faults). The experimental equipment is shown in Figure 14. The data is tested with 6205 bearings produced by SKF. The sampling frequency is 12,000 Hz. The bearing parameters are shown in Table 2.

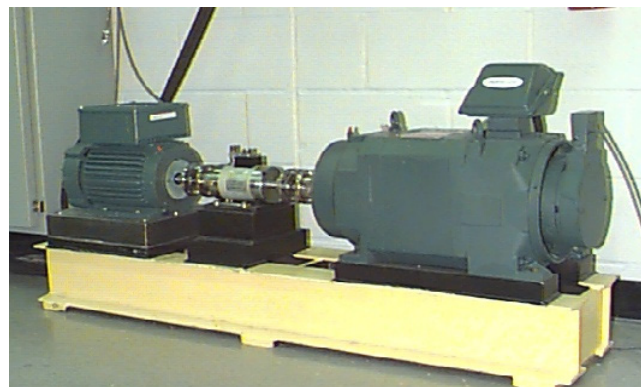


Figure 14. Experimental equipment.

Table 2. Parameters of 6205 bearings.

Number of Rolling Elements N	Ball Diameter d	Contact Angle α	Pitch Diameter D
9	7.94 mm	0	39.04 mm

In the experiment of Case Western Reserve University, the electrical discharge machining technology was used for single-point fault arrangement. The acceleration sensor is used to collect vibration signals, and the sensor is placed on the motor housing by using a magnetic switchable device. The data selected in this paper are the inner ring fault data and normal data. The method of manufacturing the inner ring fault is to arrange a pit with the size of 0.007 inches on the inner ring. The normal data are not used for any processing for the bearing. When sampling two sets of data, no load is added, and the sensor is arranged

in the six o'clock direction. Calculate the theoretical fault frequency of the bearing, and the calculation equation is shown in Equation (20):

$$\omega_{inner} = \frac{r}{60} \frac{1}{2} N \left(1 + \frac{d}{D \cos \alpha} \right) \tag{20}$$

The spindle speed of the two groups of experimental data is 1797 r/min. According to the calculation, the theoretical fault frequency of the bearing inner ring is 1019 rad/s.

The time domain diagram and frequency domain diagram of the signal are shown in Figure 15.

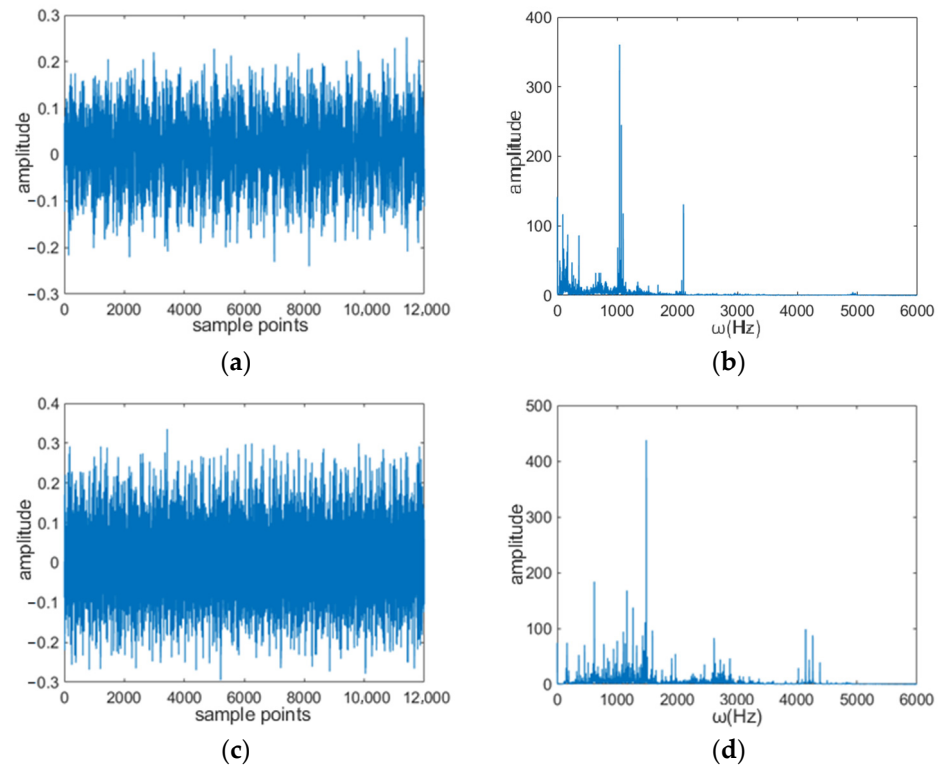


Figure 15. Time domain and frequency domain plots of experimental data. (a) Time domain diagram (normal); (b) frequency domain diagram (normal); (c) time domain diagram (inner fault); (d) frequency domain diagram (inner fault).

Figure 15 shows that the frequency component of the signal is very complex and contains a great amount of noise. It is difficult to directly identify the weak fault signal by the traditional FFT method.

The signal is normalized by energy and then decomposed by EMD. The two groups of signals are decomposed by EMD, and both obtained nine IMFs. The number of IMFs of the VMD algorithm is set to 9, and the signal is decomposed by VMD. The calculated IMF center frequency is shown in Tables 3 and 4.

Table 3. VMD decomposition results (normal).

IMF	Center Frequency (rad/s)	IMF	Center Frequency (rad/s)
IMF1	30,598.45	IMF6	6575.37
IMF2	13,208.90	IMF7	4447.15
IMF3	13,167.05	IMF8	1996.14
IMF4	9827.87	IMF9	522.98
IMF5	8262.91		

Table 4. VMD decomposition results (inner fault).

IMF	Center Frequency (rad/s)	IMF	Center Frequency (rad/s)
IMF1	26,466.81	IMF6	7579.90
IMF2	17,804.05	IMF7	5772.00
IMF3	16,318.89	IMF8	3836.90
IMF4	12,271.94	IMF9	868.91
IMF5	9311.68		

The theoretical fault frequency of the bearing is between the center frequency of IMF8 and IMF9, so IMF8 and IMF9 are added as the excitation of the double-coupled Duffing system. According to the method described in Section 4.5, 1000–1040 rad/s is selected as the frequency band to be analyzed. According to the performance parameters of the double-coupled Duffing system, the frequency band is divided into 20 parts, and the center frequency of each sub-band is taken as the built-in driving force frequency of the double-coupled Duffing system. The extracted characteristics are analyzed as the excitation, and the variation diagram of the variance jump rate of the Duffing system with the built-in driving force frequency is shown in Figure 16.

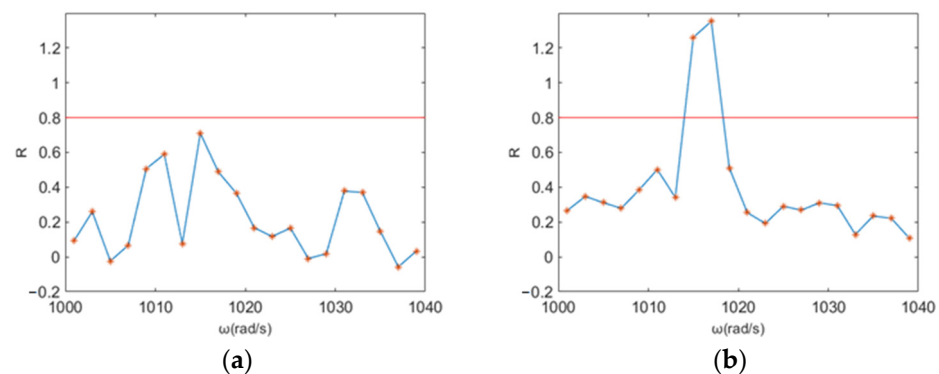
**Figure 16.** Variance jump rate change chart. (a) Normal; (b) inner fault.

Figure 16a shows that the system does not have a variance jump rate greater than the threshold value on all built-in driving force frequencies. At this time, the signal to be tested at the same frequency is not detected, which means that no fault is detected at this time. By observing Figure 16b, it can be seen that the variance jump rate exceeds the threshold of the jump rate at 1015 rad/s and 1017 rad/s. According to the evaluation criteria of Equation (4), it can be determined that the signal with the corresponding frequency has been detected, and the frequency error is small compared with the theoretical calculation, indicating that the fault has been detected. The detection results are consistent with the actual experimental conditions, indicating that this method is effective and feasible.

It is verified that the proposed method can effectively identify the weak fault signals of bearings. The research content of this paper has certain guiding significance in the field of weak fault diagnosis.

7. Conclusions

In this paper, a diagnosis method of the early weak fault of bearings based on a double-coupled Duffing system is proposed. The method has been proved to be efficient and stable by experiments. The conclusions and innovations of this paper are summarized as follows:

1. By introducing the methods of variable scale detection and phase shift detection, a new detection model of a double-coupled Duffing system is established, which makes the system more adequately meet the detection requirements in engineering applications.

2. The influence of the initial value on the system response is analyzed, and the initial value of the Duffing system is determined, which makes the system response more stable and makes the system state easier to distinguish.
3. Variance is used as a parameter to evaluate the output value of the double-coupled Duffing system. According to the variance of its output value, it can not only judge whether there is the same frequency signal but also further serve as a criterion for the detection performance of the double-coupled Duffing system. As a quantitative parameter, it has strong reliability.
4. The VMD algorithm is introduced to pre-process the data and denoise the signal. The signal after noise reduction is more conducive to the analysis of the double-coupled Duffing system, further reducing the lowest signal-to-noise ratio that the double-coupled Duffing system can detect.

In future research, we will consider introducing optimization algorithms to optimize the parameters involved in the calculation process in order to improve the algorithm's detection performance for weak fault signals.

Author Contributions: Methodology, S.S. and K.W.; validation, S.S.; resources, J.Z. and T.C.; data curation, J.Z.; writing—original draft preparation, S.S.; writing—review and editing, T.C. and Y.S. All authors have read and agreed to the published version of the manuscript.

Funding: This research received no external funding.

Institutional Review Board Statement: Not applicable.

Informed Consent Statement: Not applicable.

Data Availability Statement: This research used the published rolling bearing datasets of Case Western Reserve University. The access location of the datasets is <https://engineering.case.edu/bearingdatacenter/welcome> (accessed on 14 June 2023).

Conflicts of Interest: The authors declare no conflict of interest.

Nomenclature

Name	Abbreviation
Empirical Mode Decomposition	EMD
Empirical Wavelet Transform	EWT
Variational Mode Decomposition	VMD
Ordinary Differential Equation	ODE
Intrinsic Mode Function	IMF
Signal-to-Noise Ratio	SNR

References

1. Safaeipour, H.; Forouzanfar, M.; Casavola, A. A survey and classification of incipient fault diagnosis approaches. *J. Process Control.* **2021**, *97*, 1–16. [[CrossRef](#)]
2. Kushwaha, N.; Patel, V.N. Modelling and analysis of a cracked rotor: A review of the literature and its implications. *Arch. Appl. Mech.* **2020**, *90*, 1215–1245. [[CrossRef](#)]
3. Yan, G.X.; Chen, J.; Bai, Y.; Yu, C.Q.; Yu, C.M. A Survey on Fault Diagnosis Approaches for Rolling Bearings of Railway Vehicles. *Processes* **2022**, *10*, 724. [[CrossRef](#)]
4. Yan, R.Q.; Gao, R.X.; Chen, X.F. Wavelets for fault diagnosis of rotary machines: A review with applications. *Signal Process.* **2014**, *96*, 1–15. [[CrossRef](#)]
5. Du, T.; Zhang, H.; Wang, L. Analogue circuit fault diagnosis based on convolution neural network. *Electron. Lett.* **2019**, *55*, 1277–1279. [[CrossRef](#)]
6. Tang, S.N.; Yuan, S.Q.; Zhu, Y. Deep Learning-Based Intelligent Fault Diagnosis Methods toward Rotating Machinery. *IEEE Access* **2019**, *8*, 9335–9346. [[CrossRef](#)]
7. Wen, L.; Li, X.Y.; Gao, L. A New Two-Level Hierarchical Diagnosis Network Based on Convolutional Neural Network. *IEEE Trans. Instrum. Meas.* **2020**, *69*, 330–338. [[CrossRef](#)]
8. Zhu, W.; Wei, Y.S.; Xiao, H. Fault diagnosis of neural network classified signal fractal feature based on SVM. *Clust. Comput. J. Netw. Softw. Tools Appl.* **2019**, *22*, 4249–4254. [[CrossRef](#)]

9. Li, Z.X.; Shi, B.Q.; Ren, X.P.; Zhu, W.Y. Research and application of weak fault diagnosis method based on asymmetric potential stochastic resonance. *Meas. Control.* **2019**, *52*, 625–633. [[CrossRef](#)]
10. Borges, F.; Pinto, A.; Ribeiro, D.; Barbosa, T.; Pereira, D.; Barbosa, B.; Magalhaes, R.; Ferreira, D. An Unsupervised Method based on Support Vector Machines and Higher-Order Statistics for Mechanical Faults Detection. *IEEE Lat. Am. Trans.* **2020**, *18*, 1093–1101. [[CrossRef](#)]
11. Lai, Z.H.; Leng, Y.G. Weak-signal detection based on the stochastic resonance of bistable Duffing oscillator and its application in incipient fault diagnosis. *Mech. Syst. Signal Process.* **2016**, *81*, 60–74. [[CrossRef](#)]
12. Sun, Q.W.; Zhang, J.F. Weak signal detection based on improved chaotic oscillator system with dual coupling. *Comput. Mod.* **2012**, *1*, 17–21.
13. Li, G.H.; Cui, J.Y.; Yang, H. A New Detecting Method for Underwater Acoustic Weak Signal Based on Differential Double Coupling Oscillator. *IEEE Access* **2021**, *9*, 18842–18854. [[CrossRef](#)]
14. Wang, K.; Yan, X.P.; Yang, Q.; Hao, X.H.; Wang, J.T. Weak Signal Detection Based on Strongly Coupled Duffing-Van der Pol Oscillator and Long Short-term Memory. *J. Phys. Soc. Jpn.* **2020**, *89*, 014003. [[CrossRef](#)]
15. Cao, B.F.; Li, P.; Li, X.Q.; Zhang, X.Q.; Ning, W.S.; Liang, R.; Li, X.; Hu, M.; Zheng, Y. Detection and parameter estimation of weak pulse signal based on strongly coupled Duffing oscillators. *Acta. Phys. Sin.* **2019**, *68*, 080501. [[CrossRef](#)]
16. Dou, B.B.; Xu, M.; Peng, H.H.; Sun, K.H. Weak signal detection based on two-coupled high-order Duffing oscillator system. *Transducer Microsyst. Technol.* **2018**, *37*, 124–127.
17. Rasht, C.; Azar, N. Detecting the State of the Duffing Oscillator by Phase Space Trajectory Autocorrelation. *Int. J. Bifurc. Chaos.* **2013**, *23*, 1350065. [[CrossRef](#)]
18. Li, G.H.; Hou, Y.M.; Yang, H. A Novel Method for Frequency Feature Extraction of Ship Radiated Noise Based on Variational Mode Decomposition, Double Coupled Duffing Chaotic Oscillator and Multivariate Multiscale Dispersion Entropy. *Alex. Eng. J.* **2022**, *61*, 6329–6347. [[CrossRef](#)]
19. Fu, W.L.; Tan, J.W.; Li, C.S.; Zou, Z.B.; Li, Q.K.; Chen, T. A Hybrid Fault Diagnosis Approach for Rotating Machinery with the Fusion of Entropy-Based Feature Extraction and SVM Optimized by a Chaos Quantum Sine Cosine Algorithm. *Entropy* **2018**, *20*, 626. [[CrossRef](#)] [[PubMed](#)]
20. Hou, S.Z.; Guo, W. Optimal Denoising and Feature Extraction Methods Using Modified CEEMD Combined with Duffing System and Their Applications in Fault Line Selection of Non-Solid-Earthed Network. *Symmetry* **2022**, *12*, 536. [[CrossRef](#)]
21. Jiang, Y.; Zhu, H.; Li, Z. A new compound faults detection method for rolling bearings based on empirical wavelet transform and chaotic oscillator. *Chaos Solitons Fractals* **2016**, *89*, 8–19. [[CrossRef](#)]
22. Liang, T.; Lu, H. A Novel Method Based on Multi-Island Genetic Algorithm Improved Variational Mode Decomposition and Multi-Features for Fault Diagnosis of Rolling Bearing. *Entropy* **2022**, *22*, 995. [[CrossRef](#)] [[PubMed](#)]
23. Bix, D.L.; Pipenberg, S.J. Chaotic oscillators and complex mapping feed forward networks (CMFFNS) for signal detection in noisy environments. In Proceedings of the Proceedings IJCNN International Joint Conference on Neural Networks, Baltimore, MD, USA, 7–11 June 1992; pp. 881–888.
24. Li, G.H.; Hou, Y.M.; Yang, H. A new Duffing detection method for underwater weak target signal. *Alex. Eng. J.* **2022**, *61*, 2859–2876. [[CrossRef](#)]
25. Jin, T.; Zhang, H. Statistical approach to weak signal detection and estimation using Duffing chaotic oscillators. *Sci. China-Inf. Sci.* **2011**, *54*, 2324–2337. [[CrossRef](#)]
26. Wu, Y.F.; Huang, S.P.; Jin, G.B. Study on partial discharge signal detection by coupled Duffing oscillators. *Acta. Phys. Sin.* **2013**, *62*, 130505.
27. Zen, Z.Z.; Zhou, Y.; Hu, K. Study on partial discharge signals detection by extended Duffing oscillator. *Acta. Phys. Sin.* **2015**, *64*, 070505.
28. Dragomiretskiy, K.; Zosso, D. Variational Mode Decomposition. *IEEE Trans. Signal Process.* **2014**, *62*, 531–544. [[CrossRef](#)]

Disclaimer/Publisher’s Note: The statements, opinions and data contained in all publications are solely those of the individual author(s) and contributor(s) and not of MDPI and/or the editor(s). MDPI and/or the editor(s) disclaim responsibility for any injury to people or property resulting from any ideas, methods, instructions or products referred to in the content.